Available online at www.sciencedirect.com
ScienceDirect
Journal of Power Sources 173 (2007) 657–670
JOURNAL OF POWER SOURCES
www.elsevier.com/locate/jpowsour

Functional materials for the IT-SOFC

J. Molenda *, K. Świerczek, W. Zając

Faculty of Materials Science and Ceramics, AGH University of Science and Technology, al. Mickiewicza 30, 30-059 Kraków, Poland

Available online 26 May 2007

Abstract

The paper summarizes and discusses the basic properties of solid oxide fuel cell (SOFC) components (electrode materials and electrolyte) from the point of view of their essential functional parameters like chemical stability, transport, catalytic and thermomechanical properties under operational conditions in a SOFC. An interrelation between the defect structure of these materials related to oxygen nonstoichiometry and their electrical properties and catalytic activity was shown.

Keywords: Solid oxide fuel cells; SOFC; Electrode materials; Electrolyte

1. Introduction

A considerable interest in the fuel cells technology, observed in recent years, is related to the possibility of the direct conversion of the energy, stored within the fuels containing hydrogen, into electrical energy with the high efficiency. A relative simplicity of such devices, their high efficiency, silent work (absence of the movable mechanical parts), together with very low production of pollutants are in favor for this technology to be a future energy source. Among a wide group of the fuel cells, the solid oxide fuel cells, SOFC, are of the special interest [1–4]. The commercialization of SOFC is associated with the construction of stationary generators with powers in the range 1 kW–1 MW, although the technologically advanced papers on the application of the micro fuel cells for the portable electronic devices also have been published [5].

However, the widespread of this technology is impeded because of several factors, resulting, among others, from the properties of the electrolytes and the electrode materials. Another reason is that the reaction proceeding in the cell requires a relatively high temperature. The conductivity of an YSZ (yttria stabilized zirconia) electrolyte, currently being in use, reaches the required conductivity of oxygen ions, 10^{-1} S cm^{-1}, at around 1000 °C. The necessity of using such a high temperature causes considerable disadvantages, such as short lifetime of the cell, being a consequence of a thermal degradation and corrosion of the materials, and the side reactions occurring at the electrode/electrolyte interface. Also, it poses hindrance for the miniaturization, operational safety and low costs. Therefore, a strategic aim of the SOFC technology development is the reduction of the working temperature down to 600–700 °C. This would allow the use of cost-effective, environmentally benign materials, such as chromia-forming ferritic stainless steels, as the interconnectors or other constructing elements. In addition, thermal degradation processes are decelerated at lower temperatures and it is also possible to shorten the starting time and off-time of the generator.

For the effective performance of the SOFC at the intermediate temperatures (IT-SOFC), it is necessary to develop a new solid oxide electrolyte, characterized by a sufficiently high ionic conductivity within this temperature range (of the order 10^{-1} S cm^{-1}), and new electrode materials, working efficiently within the temperature range of 600–700 °C. The chemical stability of the electrode material, its thermomechanical properties (mutual matching of the thermal expansion coefficients, electrolyte/electrode adhesion), together with microstructural characteristics are of equal importance. For further development of the SOFC technology, it is necessary to explore the following research areas:

- The catalytic processes of the oxygen reduction and hydrogen and hydrocarbons oxidation.
- Phenomena of the ionic–electronic transport in the ceramic materials.

* Corresponding author. Tel.: +48 12 6172522; fax: +48 12 6172522.
E-mail address: molenda@uci.agh.edu.pl (J. Molenda).

0378-7753/$ – see front matter © 2007 Elsevier B.V. All rights reserved.
doi:10.1016/j.jpowsour.2007.05.085

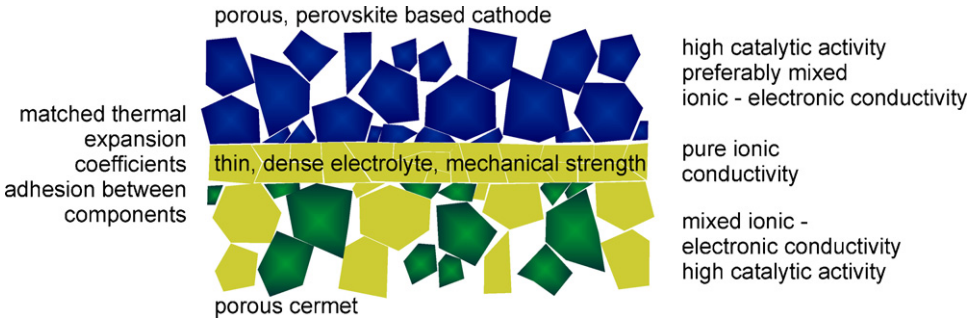

Fig. 1. The microstructure and function of SOFC components.

- Interfacial phenomena occurring at the electrode/electrolyte and interconnector/electrode interfaces.
- Nanomaterials and nanotechnologies.
- Low-temperature methods of ceramic materials preparation.
- A single chamber fuel cell.

2. Physicochemical properties and functions of the materials for SOFC cells

A schematic representation of the SOFC cell and the functions of particular components of the cell are given in Fig. 1. These functions can be considered in terms of transport and catalytic properties, as well as structural and thermomechanical ones. Electrode materials should be porous, so the cathode and anode gases could penetrate across, except for the interfacial region, in order to intensify the net diffusion of the oxygen in this area.

Cathode material: $Ln_{1-x}A_xMO_3$ oxides, where Ln = lanthanides, A = alkali-earth metals, M = Mn, Fe, Co, Ni, with perovskites structure. Such materials are mixed ionic–electronic conductors. Their ionic conductivity results from the deviation from stoichiometry in oxygen lattice (oxygen vacancies), whereas their electronic conductivity stems from a mixed valency of M^{3+}/M^{4+}, depending on the oxygen nonstoichiometry level, the amount and type of dopants. The cathode material plays the role of a catalyst in the oxygen reduction. The cathode works in the air or oxygen atmosphere, therefore in case of these oxides the problem of non-stability is practically eliminated.

Solid electrolyte: (YSZ, Ce(Gd, Sm)O_2) is a mechanically resistant, gas-tight sinter preventing fuel from a non-productive combustion. The electrolyte is in contact with the oxidizing atmosphere at the cathode side, and the highly reductive atmosphere at the anode side, where the fuel is supplied. Therefore, a model electrolyte should exhibit the ionic conductivity exclusively (with oxygen vacancies being the charge carriers) over a wide range of oxygen pressure (1–10^{-25} atm). The required ionic conductivity is about 10^{-1} S cm^{-1} at the cell working temperature. Until now, the material fulfilling the above criteria within the temperature range 600–700 °C has not been found.

Anode material: a Ni/YSZ cermet or Ni/Ce(Sm, Gd)O_2 is a mixed ionic–electronic conductor. The ionic conductivity is associated with oxygen vacancies in YSZ or Ce(Sm, Gd)O_2. The electronic conductivity is related to a conductive percolation path that is formed in the anode material containing about 30% wt. of metallic Ni. Conveniently, nickel works as a catalyst for the oxidation of fuel. A highly reductive atmosphere at the anode is safe for the anodic material and, in addition, improves its effectiveness by preserving the catalytically active form of nickel and increasing the electronic conductivity in CeO_2.

All components of the cell should exhibit both chemical and thermal compatibility.

2.1. Electrolyte materials

Fig. 2 presents the temperature dependence of the ionic conductivity of different solid oxide electrolytes with the fluorite (this structure is considered to be remarkably suitable for a high ionic conductivity), perovskite, brownmillerite and apatite-type structures. These materials are the potential candidates for the electrolyte in SOFC cells.

2.1.1. ZrO_2-based electrolytes

Stabilized zirconia is a commonly known and widely used solid oxide electrolyte, stable within a wide range of both reducing and oxidizing atmospheres [4,6]. Pure ZrO_2 at room temperature has a monoclinic structure, which above 1170 °C transforms to a tetragonal, and, as the temperature increases above 2370 °C, to cubic fluorite structure. The cubic phase exists

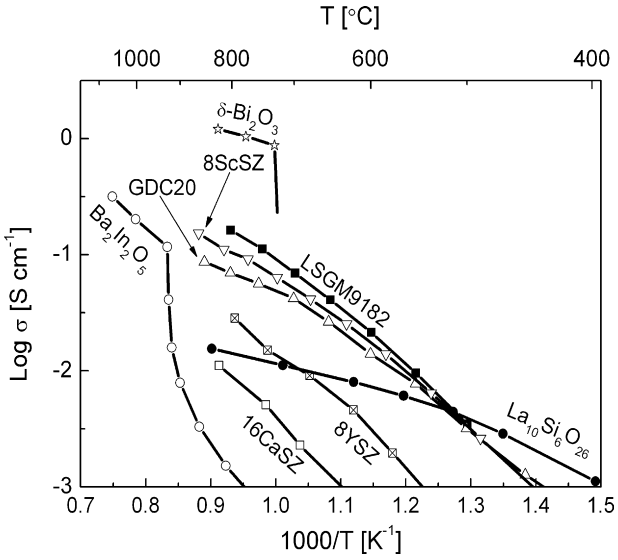

Fig. 2. The ionic conductivities of the chosen oxide electrolytes [7–13].

up to the melting point at 2680 °C. The stabilization of the cubic structure within a wide temperature range (from room temperature to melting point) is possible, when appropriate aliovalent oxides are used as dopants. Simultaneously, the dopants give rise to the ionic conductivity of zirconia.

Clearly, a thermal stability of zirconia is related to the size of Zr^{4+} ions. These ions seem to be too small to maintain the cubic fluorite structure, where there are eight coordinated oxygen ions (in the case of monoclinic structure there are six oxygen ions). The addition of the rare earth ions stabilizes the cubic structure by creating oxygen vacancies. The vacancies are gathered around Zr^{4+} more likely than around the doping ions, and the effective number of the coordinated oxygen ions is about 6 or 7.

Undoped zirconia exhibits the deviation from stoichiometry with the oxidant deficiency (oxygen vacancies, ZrO_{2-y}). The defect formation is given according to the reaction:

$$O_O{}^x = 1/2O_2 + V_O{}^{\bullet\bullet} + 2e^- \quad (1)$$

If a complete ionization of defects is assumed (doubly ionized oxygen vacancies $V_O{}^{\bullet\bullet}$), then the equilibrium constant for the reaction (1) and lattice electroneutrality condition are as follows:

$$K = [V_O{}^{\bullet\bullet}][e^-]^2 pO_2{}^{1/2} \quad (2)$$

$$[e^-] = 2[V_O{}^{\bullet\bullet}] \quad (3)$$

By solving the Eqs. (2) and (3) one can obtain the following characteristic relations between the concentration of the ionic and electronic defects and the oxygen partial pressure:

$$[V_O{}^{\bullet\bullet}] \sim pO_2{}^{-1/6} \quad (4)$$

and

$$[e^-] \sim pO_2{}^{-1/6} \quad (5)$$

It can be found from Eq. (1) that oxygen nonstoichiometry introduces the electronic charge carriers, the concentration of which is directly proportional to the oxygen vacancies concentration (2:1). As a consequence, a pure zirconium dioxide is not an electrolyte, but is an electronic conductor, because the mobility of the electronic charge carriers is few orders of magnitude higher than the mobility of ionic defects.

However, by doping with metal ions of the valency lower than +4 and appropriate sizes one can obtain zirconia with a stabilized structure and the properties of a solid electrolyte. For example, CaO (15%) is incorporated in ZrO_2 according to the reaction:

$$CaO \overset{ZrO_2}{=} Ca''_{Zr} + V_O{}^{\bullet\bullet} + O_O^x \quad (6)$$

As can be seen, Zr^{4+} ions are replaced with Ca^{2+} ions. The net electroneutrality requires one oxygen vacancy per each Ca^{2+} ion. Thus, the increasing amount of Ca^{2+} is followed by the growing concentration of the oxygen vacancies. This, in turn, leads to a decrease in the electron concentration, so that the reaction constant (Eq. (2)) remains unchanged at a given temperature. The electroneutrality condition for this case can be expressed as

$$p + 2[V_O{}^{\bullet\bullet}] = n + 2[Ca''_{Zr}] \quad (7)$$

The following simplified electroneutrality conditions can be taken into account:

1. At very low oxygen partial pressures—the dominating defects are related to the nonstoichiometric reaction (1). If $[V_O{}^{\bullet\bullet}] \gg [Ca''_{Zr}]$, then the electroneutrality condition is given by

$$n = 2[V_O{}^{\bullet\bullet}] \quad (8)$$

2. For high oxygen partial pressures—the concentration of the defects connected with the deviation from stoichiometry (i.e. $V_O{}^{\bullet\bullet}$ and electrons) is low. It is possible that the electronic holes would compensate the concentration of the dopant:

$$p = 2[Ca''_{Zr}] \quad (9)$$

3. At moderate oxygen partial pressures (the electrolyte properties regime)—the concentration of the oxygen vacancies is controlled by the concentration of the dopant:

$$[V_O{}^{\bullet\bullet}] = [Ca''_{Zr}] \quad (10)$$

4. The intrinsic regime—where n = p, is impossible, because of a wide energy band gap of ZrO_2 (4.5 eV) and high concentration of the dopant (15 at.%).

A schematic representation of the relationship between the concentration of the ionic and electronic defects and oxygen partial pressure for the ZrO_2–15 at.% CaO system is shown in Fig. 3. The interesting regime of the moderate oxygen partial pressures, where $[V_O{}^{\bullet\bullet}] = [Ca''_{Zr}]$, that is where zirconia exhibits the properties of a solid oxide electrolyte is remarkably wide.

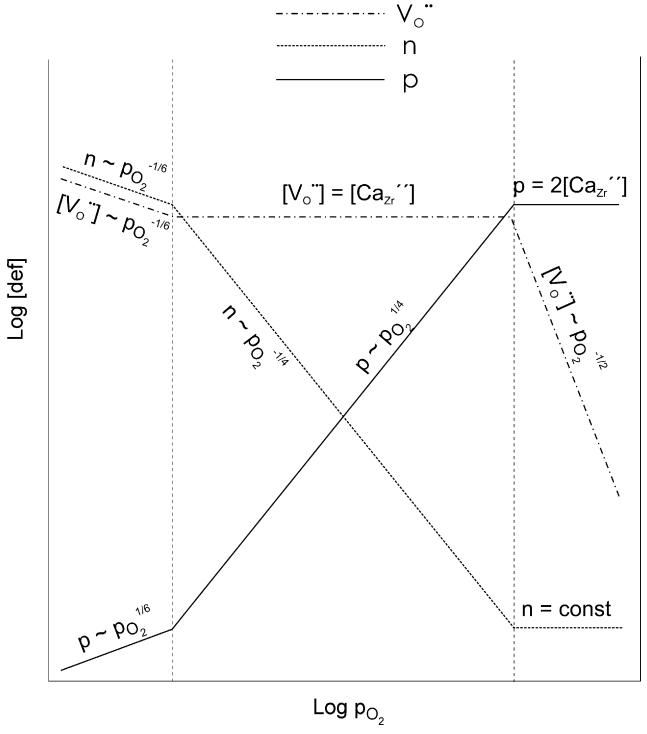

Fig. 3. A schematic dependencies of the ionic and electronic defects as a function of the oxygen partial pressure for the ZrO_2–15 at.% CaO system.

For example, at the temperature of 1200 °C zirconia acts as a solid electrolyte at the oxygen partial pressure within the range of 37 orders of magnitude, i.e. from 4×10^{6} to 6×10^{-31} atm.

YSZ—*yttrium-stabilized zirconia* is stable within a slightly narrower range of the oxygen partial pressures, as compared with CaSZ. Nevertheless, this range is still sufficient for the SOFC applications. In addition, YSZ shows higher ionic conductivity (Fig. 2). There are many benefits accruing from the application of the solid electrolytes based on doped zirconia, as these materials exhibit good mechanical properties. Still, the construction of a cell, where the denser layer of the electrolyte works as a support, requires high mechanical resistance; therefore the electrolyte layer must be at least about a hundred micrometer thick. Consequently, with the increasing thickness of the electrolyte layer the internal electric resistance of the cell also increases, leading to a drop in the effective power of the cell.

The major disadvantage of these electrolytes is their insufficiently high ionic conductivity within the temperature range of 600–700 °C. Among the electrolyte materials based on the zirconia doped with rare-earth elements the highest ionic conductivity is acquired for the system 11 at.% Sc_2O_3–ZrO_2. The ionic conductivity of the 11 at.% Sc_2O_3–ZrO_2 is about 0.15 S cm^{-1} at 800 °C, therefore is similar to those obtained for 8YSZ at 1000 °C [14]. Such high values result from small distortions introduced into the crystal lattice by the Sc^{3+} ions (0.87 Å), substituting the Zr^{4+} (0.84 Å). Fig. 4 presents how the ionic radii of the dopants affect the value and the activation energy of electrical conductivity of zirconia [14,15]. An increase of the ionic radius of the dopant stabilizes the fluorite structure of zirconia, decreases the conductivity of oxygen vacancies and concomitantly increases the activation energy of the conductivity. Still, the application of scandium oxide carries several disadvantages, such as high cost of this material, ageing processes occurring at high temperatures for the dopant concentration higher than 10 at.% and difficulties in obtaining a dense sinter [16,17].

There are two possible approaches to improve the electrical conductivity of the zirconia-based electrolyte. One requires a further development of the fabrication techniques of thin, gas-tight YSZ layers [18]. Another approach is to modify the microstructure of the zirconia, e.g. by introducing a small amount of Al_2O_3 that changes the properties of the grain boundaries, by facilitating the sintering process and the total electrical conductivity of the electrolyte [19].

2.1.2. CeO_2-based electrolytes

Electrolytes based on cerium dioxide (e.g. GDC – gadoline doped ceria, SDC – samarium doped ceria) have a fluorite structure, similarly to yttria-stabilized zirconia. Fortunately, the size of Ce^{4+} ions is sufficient (0.97 Å) to form a stable fluorite structure, therefore the oxygen vacancies which are created after introducing the dopant, are more likely to gather around the dopant ions rather than around the cerium ions. As a result, the conductivity increases, whereas the activation energy decreases (Fig. 2).

Pure ceria, likewise the undoped zirconia, is characterized by a deviation from stoichiometry in the oxygen sublattice (oxygen vacancies, CeO_{2-y}, see Eq. (1)). By way of analogy, it is not a solid electrolyte, but practically an electronic conductor. Introducing the aliovalent ions into cerium dioxide is followed by formation of the oxygen vacancies; this leads to the increase in the ionic conductivity. A process of incorporating the trivalent ions of the dopant is described by the reaction:

$$CeO_2 + R_2O_3 \rightarrow Ce_{Ce}^{X} + 2R'_{Ce} + 5O_O^X + V_O^{\bullet\bullet} \quad (11)$$

Usually the rare-earth oxides and Y_2O_3 play the role of the dopant, however, it is also possible to use alkali-earth metal oxides. Interesting results were obtained when, apart from the rare-earth metal oxides, small amounts (of the order of 1 at.% of the alkali metal oxides (Li_2O, Cs_2O) were present in the ceria matrix [20,21]. Fig. 5 illustrates the electrical conductivity of the electrolyte as a function of the ionic radius of the dopant. A distinct maximum of the electrical conductivity is clearly visible for the dopant with the ionic radius greater than Ce^{4+}. The maximum appears for divalent and trivalent ions of the dopant. The ions giving the most significant rise in the conductivity cause the smallest change in the lattice parameters, as compared with the undoped CeO_2. As can be seen in Fig. 5 samarium and gadolinium ions are the most promising candidates for the dopants.

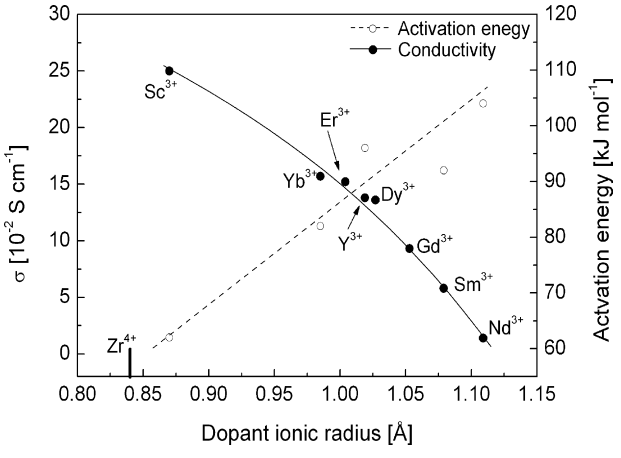

Fig. 4. The influence of the ionic radii of the dopant on the ionic conductivity and the activation energy for ZrO_2-based electrolytes. Data taken from [14,15].

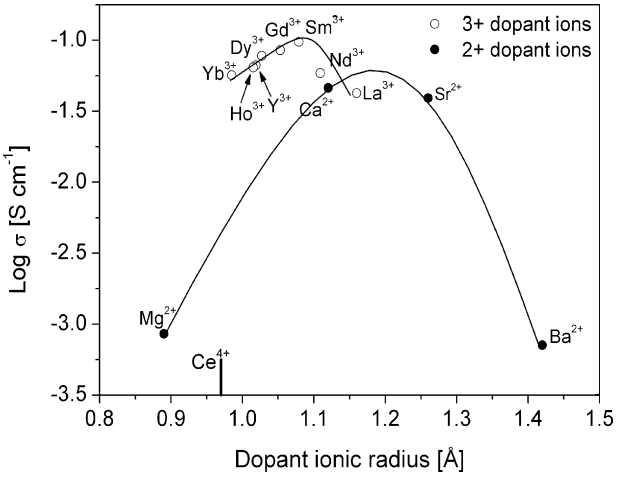

Fig. 5. The influence of the ionic radii of the dopants over the ionic conductivity of the CeO_2 based electrolytes [22–24].

The qualitative description of the changes in the ionic conductivity of ceria-based electrolytes is similar for different dopants. A characteristic maximum, appearing between 10 and 20 at.% of the dopant is observed [20,25]. This behavior arises from the formation of the associated point defects $\{Sm_{Ce}–V_O^{\bullet\bullet}\}^{\bullet}$ when the concentration of a dopant exceeds a certain value. As a consequence, the mobility of oxygen vacancies decreases. There is a minimum in the activation energy for the concentration of Sm, which is accompanied by a maximum on the conductivity of the electrolyte. A certain rise in the conductivity can be achieved, if samarium ions together with gadolinium ions [26] or a greater number of the dopants are introduced concurrently into the ceria lattice [21,27].

The application of the ceria-based electrolytes is impeded mainly because of an increase in the electronic conductivity in reducing environments. Taking into consideration the structure of the ionic defects in $Ce_{1-x}Gd_xO_{2-x/2}$ electrolyte, one can see that the range of the oxygen partial pressure, where the electrolyte is a purely ionic conductor, is much narrower ($1–10^{-8}$ atm), as compared with the zirconia-based electrolytes, as it was shown previously. The presence of the electronic component of the conductivity of ceria originates from a stable valency of Ce^{3+} in a fluorite type structure and can be explained on the basis of first-principles quantum mechanical simulations [28]. Conversely, the Zr^{3+} is not stable in the fluorite type structure. The behavior of ceria dioxide in reducing atmospheres can be described with a model of the reversible $CeO_2–Ce_2O_3$ reduction mechanism [28]. In CeO_2, 4 valence electrons of cerium ($6s^25d^14f^1$) are transferred to the 2p band of oxygen, while in Ce_2O_3 one electron of cerium remains on the Ce f^1 level. The density of states calculations for CeO_2 indicate that there is an empty, narrow band Ce f^0, located in the energy band gap between the valence band and the conductivity band (Fig. 6). The elementary stage of the reduction process of CeO_2 to Ce_2O_3 ($CeO_{1.5}$) is the formation of a single oxygen vacancy. The FP-LMTO-GGA (Full Potential Linear Muffin Tin Orbitals Generalized Gradient Approximation) calculations revealed that, energetically, the formation of the oxygen vacancy is most favorable in the proximity of two Ce^{3+} ions (0.26 eV as compared with 4.55 eV for the perfect crystal). This, in turn, would lead to the formation of $2Ce^{3+}–V_O^{\bullet\bullet}$ associates. The formation of an oxygen vacancy is drawn schematically in Fig. 6. In reductive environments oxygen atoms are released from the CeO_2 crystal, leaving two electrons, which are localized on the f level of two neighboring cerium ions. Concomitantly, the ceria ions Ce^{4+} are converted into Ce^{3+} (Fig. 6) and the oxygen vacancy is formed. Oxygen diffuses from the bulk to the surface of the crystal, which is tantamount to the diffusion of the oxygen vacancies to the crystal interior. Electrons follow the oxygen vacancies and localize in their proximity; as a result, the Ce^{3+} states are formed uniformly across the volume of the crystallites and are responsible for electronic component of conductivity. The reduction process of CeO_2 at low oxygen partial pressures can be regarded as the formation of complex defects $Ce^{3+}–V_O^{\bullet\bullet}$, their movement and ordering.

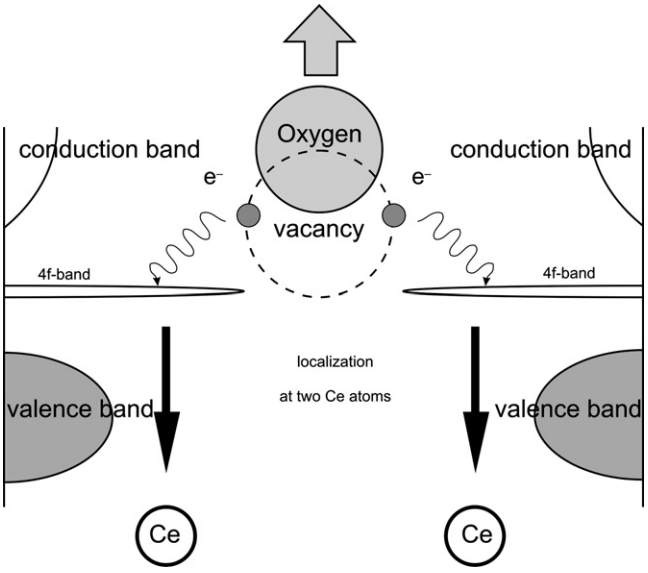

Fig. 6. The process of an oxygen vacancy formation in ceria [28].

Two different approaches to this problem were proposed. One is to cover the CeO_2 electrolyte at the anodic side with a protective layer, e.g. $BaCe_{1-x}Sm_xO_{3-\alpha}$ [29] or YSZ [30]. The second approach is to introduce several different dopants instead of one, which in turn leads to the improved stability to reductive atmospheres [21]. A simultaneous doping of the materials from CeO_2–Sm system with Li, Cs or Ca ions causes the increased degree of disorder in the system and the decrease of the bonding energy of the dopant-oxygen vacancy associates. As a result, the ionic conductivity is improved and the electrolytic range is shifted towards more reductive atmospheres (10^{-14} atm).

The electrical conductivity of CeO_2-based materials is strongly affected by the so-called space charge effect. Therefore, if the grain size approaches a nanometric scale, the electronic component of the conductivity becomes more significant and the dominating charge carriers are changed from ions to electrons [31,32]. For the zirconia electrolyte an inverse situation occurs, where a decrease in grain size results in the enhancement of the ionic conductivity and the improvement of parameters of the electrolyte [33]. The investigations [32] confirmed that the transition to a nanometric scale for the cerium dioxide leads to a decrease in the energy band gap. The donor levels, resulting from the deviation from stoichiometry in oxygen sublattice, become shallower and the electronic component of conductivity appears. Certainly, these facts should be taken into account when fabricating the materials with the grains of a nanometric size or in very thin layers.

Another approach to maximize the ionic conductivity the electrolyte is creation of "sandwich-like" structures with very thin (30–50 nm) alternating layers of two different ionic conductors. In case of optimized $(Ce, Sm)O_2–CeO_2$ superlattice [34,35] over an order of magnitude increment of ionic conductivity in relation to single thin film was presented.

2.1.3. Bi_2O_3

The δ phase of Bi_2O_3, occurring within the temperature range of 729–825 °C exhibits one of the highest oxygen conductivity among all the materials investigated so far (Fig. 2). Since

the phase exists only within a narrow range of temperature and is susceptible to reduction in non-oxygen atmospheres into metallic bismuth, the unmodified Bi_2O_3 is not applied as the electrolyte for high temperature fuel cells.

2.1.4. $LaGaO_3$-based electrolytes

The materials based on $LaGaO_3$ with the perovskite structure are potential electrolyte materials, due to their remarkably high oxygen ion conductivity [36] (Fig. 2). In particular, $La_{0.9}Sr_{0.1}Ga_{0.8}Mg_{0.2}O_{3-\delta}$ is commonly referred to as an excellent electrolyte material. The ionic conductivity of these materials is few orders of magnitude higher than YSZ. However, a successful implementation of the $LaGaO_3$ for the commercial applications requires a further improvement of their chemical stability. Under the cell operating conditions two adverse effects are observed: at the interface between the electrolyte and the anode the compound that contains nickel–$LaNiO_3$ is formed, negatively altering the cell performance [37]. Secondly, at the temperatures higher than 800 °C, under the reductive atmospheres, $LaGaO_3$ decomposes, due to a high volatility of Ga_2O_3 [38]. Although the application of this material has some disadvantages, it has been implemented in SOFC cells with the powers up to 3.5 W cm^{-2}. In these cells the composite electrolytes were used, comprising of LSGM layer covered with a thin film of CeO_2 doped with Sm [39].

2.1.5. New potential electrolyte materials

Apart from the oxides with a fluorite or perovskite structures, other oxide materials are also taken onto consideration for the application as an electrolyte for SOFC. The compounds with apatite structure described by a general formula $A_{10}(MO_4)_6O_{2\pm y}$ (A = rare-earth or alkaline-earth ions, M = Si, Ge, P, V) may serve as an example. Among the examined compounds $La_{10}(SiO_4)_6O_{2\pm y}$ exhibits one of the highest electrical conductivities (1.08×10^{-2} S cm^{-1} at 700 °C, Fig. 2), with the transference number of the oxygen ions close to one. Even though the properties of these oxides are inferior to other materials at the temperatures above 600 °C, their ionic conductivity decreases rather slowly with the decreasing temperature and gradually becomes higher than the conductivities of other electrolytes below 500 °C. A plausible explanation behind the oxygen ion conductivity is the interstitial mechanism, resulting from the excess of oxygen [40,41]. A characteristic feature of this group of compounds is the possibility of various modifications of their properties by doping with different ions. The main drawback arises from the difficulty in obtaining dense sinters and a change in the mechanism of ionic conductivity, resulting from the change of dominating defects type (from interstitial oxygen ions to oxygen vacancies); this in turn leads to a decrease in the ionic conductivity.

Another group of the materials showing a high conductivity of the oxygen ions are the compounds with the structure of a brownmillerite type [13,42,43]. This structure can be derived from a perovskite structure, if a 1/6 of the oxygen atoms is removed and exchanged with the ordered oxygen vacancies. $Ba_2In_2O_5$ serves as a typical example of the compounds of the brownmillerite structure. These compounds undergo an order–disorder transformation at about 800 °C, which is associated with the location of oxygen vacancies on the atomic planes [1 0 1]. The material could be competitive as compared to other electrolytes for SOFC, under the condition that a transition temperature would be reduced. This can be achieved by incorporating the dopant both into Ba and In sublattice [13]. It can be seen that at low temperatures $Ba_2In_2O_5$ absorbs water; as a result, the protonic conductivity occurs. This gives an opportunity for the application of this material in SOFC as a protonic electrolyte.

2.2. Cathode materials

In classical SOFC with a zirconia-based electrolyte, working at 1000 °C, a $La_{1-x}Sr_xMnO_3$ oxide plays the role of the cathode. This compound is of a perovskite structure and is usually referred to as LSM. LSM is characterized by a high, practically purely electronic conductivity. However, at lower temperatures, the efficiency of LSM cathode is significantly decreased. Therefore, a new class of the cathode materials enabling the reduction of the SOFC operating temperature down to 600 °C is at the focal point of the vast number of researchers. Among a wide group of materials which are potentially useful for this purpose, the majority of them crystallize in perovskite structure [44]. This type of the structure, together with its derivatives is often characterized by the presence of a rhombohedral or tetragonal lattice distortion. It is also responsible for the effective transport of electrons, owing to the overlapping 3d orbitals of the transition metal in an octahedral position with 2p orbitals of oxygen atoms. The ionic transport is also possible and it occurs via oxygen vacancies. The possibility of a high, mixed ionic–electronic conductivity of some of the perovskites is highly desirable, because it may improve the effectiveness of the cathode performance in SOFC within the lower temperature range. The mechanism of the processes, occurring at the electrolyte/electrode interface when the electrode material shows only an electronic conductivity (e.g. in LSM), is presented in Fig. 7a. Three elementary stages can be distinguished:

1. The adsorption of oxygen at the active centers on the surface of the cathode material.
2. A surface diffusion process of the adsorbed oxygen towards a three-phase boundary (*tpb*; electrolyte/electrode/oxygen).
3. The reaction of incorporation/reduction of the adsorbed oxygen to a lattice oxygen ions.

Because of the absence of the conductivity via oxygen ions in the cathode material, the oxygen reduction is restricted to a one-dimensional three-phase boundary *tpb*. In practice, the reaction is spread out over a few nanometers area from the *tpb*. This leads to a "bottle neck" effect, leading in turn to considerable limitations of power output of the SOFC. It is possible to decrease the cathode polarization (i.e. the reduction of electrical losses related to the cathode processes) of the SOFC, if the length of a *tpb* is increased. This can be done by tailoring the microstructure of the composite, comprising of the electrode and the electrolyte. However, in order to achieve the acceptable

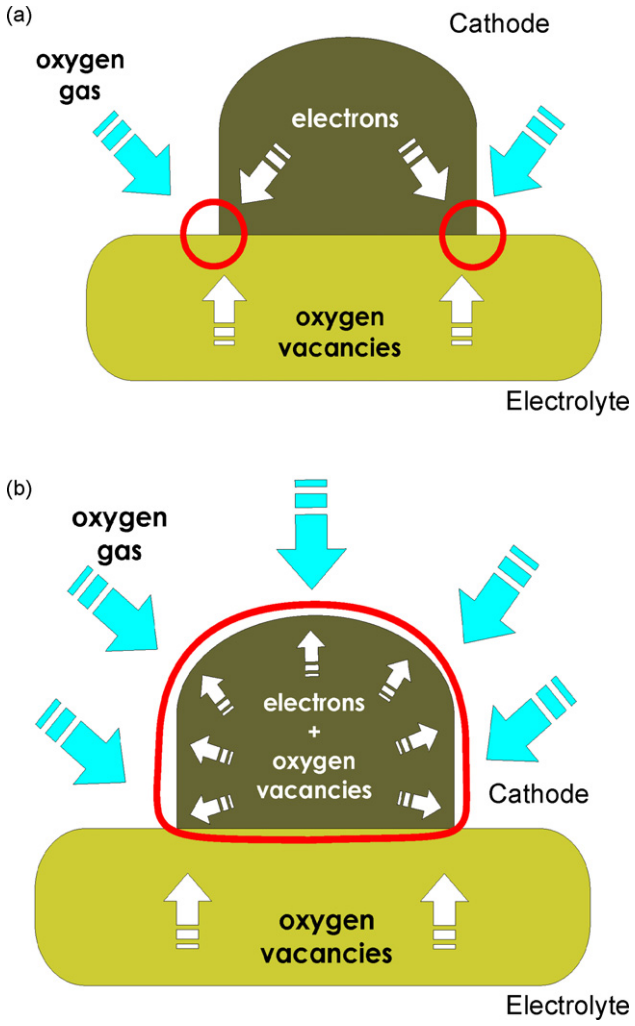

Fig. 7. Schematics of electrode processes occurring at the electrolyte/cathode material interface. (a) In case of pure electronically conductive cathode material. (b) In case of mixed ionic–electronic conductivity of the cathode material.

polarizations at lower temperatures, a different approach must be taken.

A crucial factor for IT-SOFC cells is the implementation of the perovskite material, characterized by the improved ionic–electronic transport for a cathode. This is associated with a more complex chemical composition and a disordered structure in a sense of a perfect long-range order [45] that often leads to a strongly correlated transport mechanism of oxygen and peculiar functional properties. Many perovskites exhibit large flexibility of the structure, resulting in a bewildering variety of physicochemical properties and are frequently referred to as "inorganic chameleons". The materials characterized by a high mixed ionic–electronic conductivity can be obtained by changing the chemical composition, which results in a completely different mechanism of the cathode processes (Fig. 7b). Apart from the electrode reaction that occurs for LSM and is related to *tpb*, the competitive processes occur, namely the incorporation and reduction of the adsorbed oxygen at the oxygen vacancies sites on the entire surface of the cathode material. The lattice oxygen diffuses towards the electrolyte via oxygen vacancies, across the whole volume of the cathode material, leading to the enhancement of these processes (Fig. 7b).

Two major groups of compounds with a perovskite structure can be classified as potential materials for SOFC operating within the temperature range of 600–700 °C: $Ln_{1-x}Sr_xCo_{1-y}Fe_yO_{3-\delta}$ (where Ln – e.g. La, Sm, Nd, Gd, Dy) [46–52] and $Ln_{1-x}A_xM_{1-y}Mn_yO_{3-\delta}$ (where Ln – e.g. La, Nd, Pr; A – Ca, Sr; M – a 3d metal other than Mn) [53,54]. Also, the compounds: $La_{1-x}Sr_xNi_{1-y}Fe_yO_{3-\delta}$ [55,56] and $LaNi_{1-y}Co_yO_{3-\delta}$ [57] are currently under examinations. The compounds of LSCF group are based on strontium-doped $LaCoO_{3-\delta}$, which shows a quite high ionic–electronic conductivity up to 650 S cm^{-1} at 800 °C. This material, however, exhibits a relatively high coefficient of thermal expansion, much higher than the coefficients of the electrolyte materials suitable for the application in SOFC (i.e. GDC, LSGM, YSZ). Thermal expansion coefficients of the materials from $La_{1-x}Sr_xFeO_{3-\delta}$ group are considerably low and close to those of the electrolytes; still, their conductivity is not satisfying. Nonetheless, it is possible to combine the benefits of those materials when using mixed perovskites LSCF, although there is a general disagreement in the literature on the optimal composition of Co:Fe and La:Sr [46,47,58]. The compounds of the $LaNi_{1-y}Co_yO_{3-\delta}$ type seem to be promising materials owing to their metallic conductivity. However, these materials show notably lower thermal stabilities. Also, in this case the influence of nickel on the ionic conductivity of the material is not fully apprehended. On the other hand, the compounds described by a general formula $LaNi_{1-y}Fe_yO_{3-\delta}$ appear to be particularly attractive for this application, since they exhibit a comparatively high electrical conductivity and suitably low thermal expansion coefficient.

$Ba_{1-x}Sr_xCo_{1-y}Fe_yO_{3-\delta}$ (BSCF) [59] shows interesting properties and is successfully implemented for a prototype single chamber fuel cell [60,61]. Outstandingly high powers of over 1300 mW cm^{-2} are achieved at 600 °C using porous $Ba_{0.5}Sr_{0.5}Co_{0.8}Fe_{0.2}O_{3-\delta}$ cathode and dense 10 μm $Gd_{0.1}Ce_{0.9}O_{1.95}$ [62] or even higher (over 1900 mW cm^{-2} at 600 °C) using $Sm_{0.6}Sr_{0.4}CoO_{3-\delta}$ fabricated on the surface of 5 μm LSGM electrolyte with 400 nm thick SDC buffer layer [39].

An important aspect, yet not completely understood, is the presence of 3d cations on a high oxidation state in the cathode material. These ions are capable of catalyzing the cathode reactions, considerably augmenting the effectiveness of cathode performance [63–65].

A microscopic mechanism of the catalytic process of the oxygen reduction has not been yet entirely explored. It has been established that the rate of the oxygen adsorption on the cathode material depends on the concentration of oxygen vacancies and quasi-free electrons in the cathode. A deviation from stoichiometry towards the oxygen deficiency introduces defect centers, the ionization of which leads to a change in the concentration of charge carriers. Therefore, the oxygen nonstoichiometry and the presence of dopants shift the position of the Fermi level [66,67], which, according to the electronic theory of catalysis is a vital factor for catalytic activity of the cathode material. The magnitude of the oxygen nonstoichiometry is related to the synthesis

conditions (i.e. temperature, the oxygen partial pressure) and the type and concentration of the dopant [68–71].

In order to examine the mechanism of the oxygen reduction, in this paper a complex studies over the structure of the ionic and electronic defects, resulting from the deviation from stoichiometry or doping with different ions, are carried as a function of the temperature and the oxygen partial pressure. The results allow for the design of the functional properties of perovskite-type oxides—the perspective cathode materials of a high electrochemical effectiveness for IT-SOFC.

Fig. 8 presents the temperature dependence of the electrical conductivity and the thermoelectric power for chosen perovskites from the LSCF group: $La_{0.8}Sr_{0.2}Co_{0.2}Fe_{0.8}O_{3-\delta}$ and $La_{0.6}Sr_{0.4}Co_{0.2}Fe_{0.8}O_{3-\delta}$ measured in air. For the base oxide $LaCo_{0.2}Fe_{0.8}O_{3-\delta}$, the ions of cobalt and iron are in Co^{3+} ($3d^6$) and Fe^{3+} ($3d^5$) states. By substituting 0.2 mole of La^{3+} with Sr^{2+} in $La_{0.8}Sr_{0.2}Co_{0.2}Fe_{0.8}O_{3-\delta}$, the valency of a Co^{3+} ions is increased to Co^{4+}. A qualitative, schematic representation of the

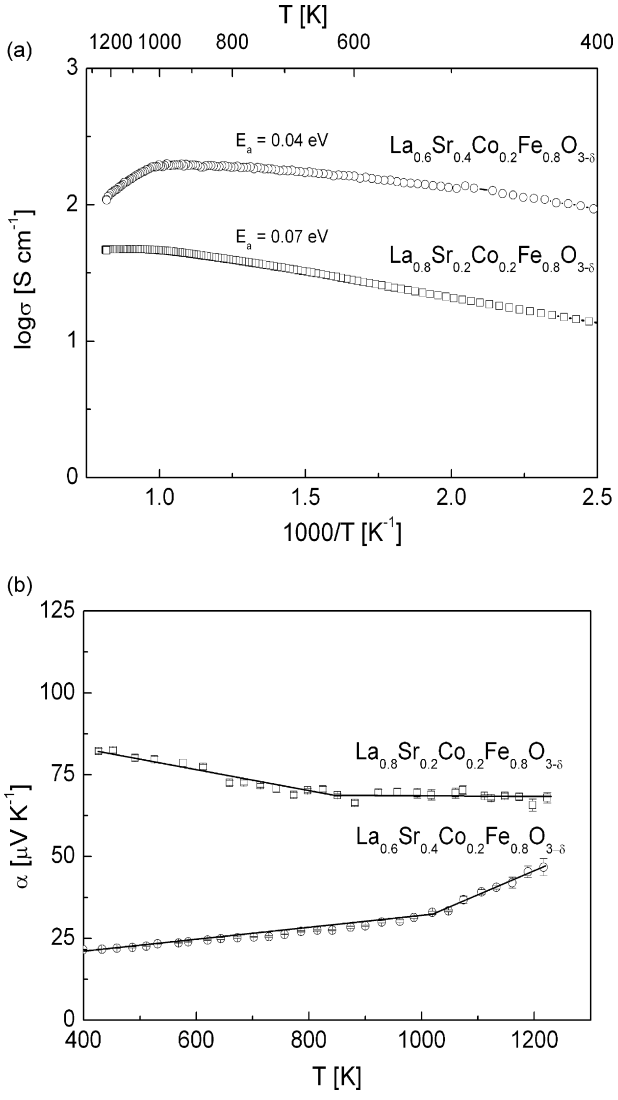

Fig. 8. Temperature dependence of (a) the electrical conductivity and (b) the thermoelectric power of $La_{0.8}Sr_{0.2}Co_{0.2}Fe_{0.8}O_{3-\delta}$ and $La_{0.6}Sr_{0.4}Co_{0.2}Fe_{0.8}O_{3-\delta}$ measured in air.

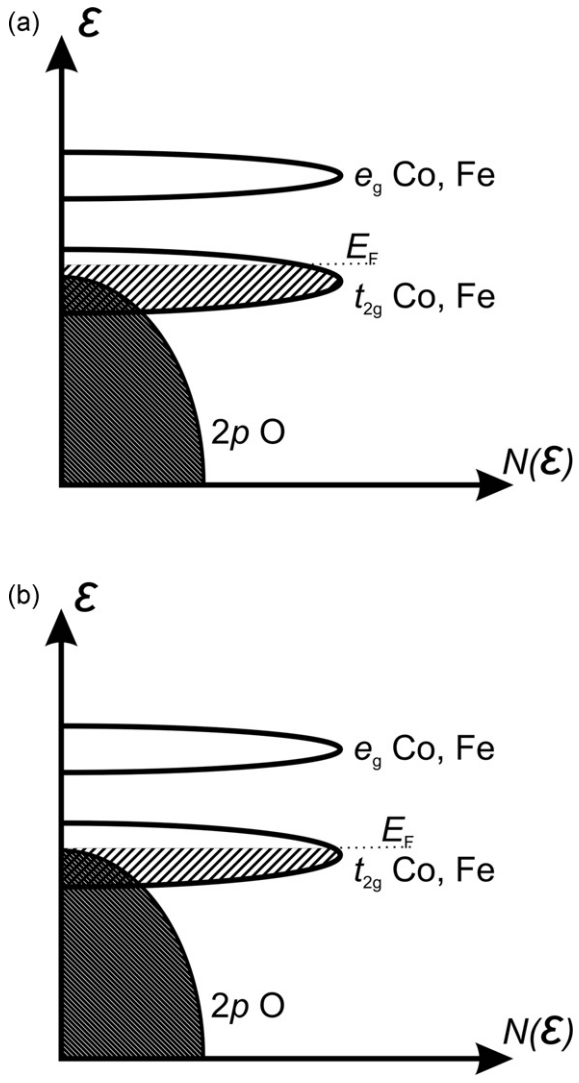

Fig. 9. Schematic representation of the electronic structure of the (a) $La_{0.8}Sr_{0.2}Co_{0.2}Fe_{0.8}O_{3-\delta}$ and (b) $La_{0.6}Sr_{0.4}Co_{0.2}Fe_{0.8}O_{3-\delta}$ perovskites.

electronic structure of the $La_{0.8}Sr_{0.2}Co_{0.2}Fe_{0.8}O_{3-\delta}$ perovskite is shown in Fig. 9a. The observed electronic properties of this perovskite (Fig. 8) can be explained in terms of this model. According to the model a charge transport proceeds in a narrow band t_{2g} (Co, Fe) via localized states (electronic holes), with energies close to Fermi energy. The resulting activation energy of the conductivity (Fig. 8a) is close to 0.07 eV and is identified with the activation energy of the holes movement in the narrows t_{2g} band. The increasing strontium content in the lanthanum sublattice up to 0.4 mol for the $La_{0.6}Sr_{0.4}Co_{0.2}Fe_{0.8}O_{3-\delta}$ composition additionally increases the average valency of iron (therefore Co^{4+}, Fe^{3+}, Fe^{4+} are present) and leads to the enhancement of the conductivity of one order of magnitude. As a result, the thermoelectric power characteristic is typical for metallic properties (Fig. 8b). This behavior can be ascribed to lowering of the Fermi level into a t_{2g} band, resulting from the increased strontium content (the t_{2g} electron concentration is diminished as the iron valency increases). Consequently, the Fermi level is shifted into a much broader O 2p band (Fig. 9b).

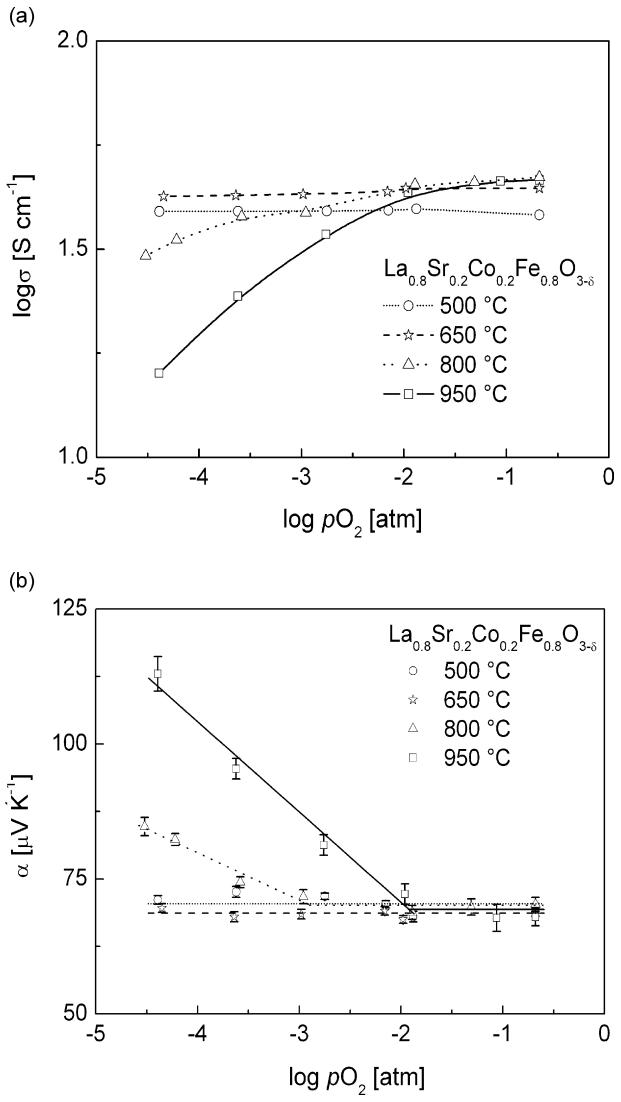

Fig. 10. Equilibrium dependences of (a) the electrical conductivity and (b) the thermoelectric power of $La_{0.8}Sr_{0.2}Co_{0.2}Fe_{0.8}O_{3-\delta}$ as a function of the oxygen partial pressure at 500, 650, 800, 950 °C.

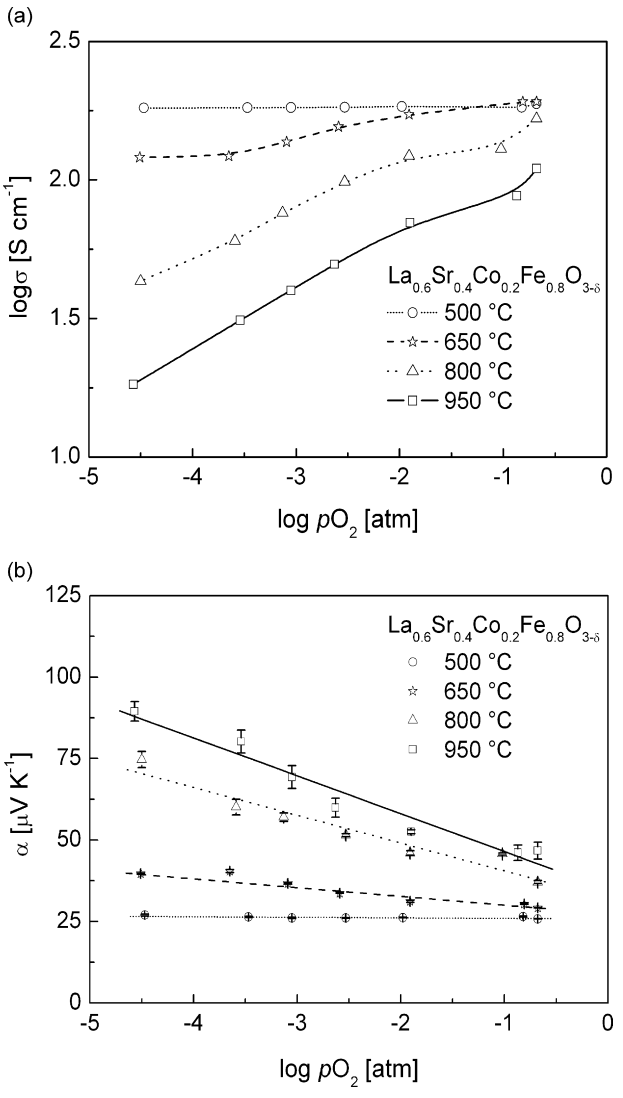

Fig. 11. Equilibrium dependences of (a) the electrical conductivity and (b) the thermoelectric power of $La_{0.6}Sr_{0.4}Co_{0.2}Fe_{0.8}O_{3-\delta}$ as a function of the oxygen partial pressure at 500, 650, 800, 950 °C.

The observed drop in the electrical conductivity above about 730 °C for both compositions $La_{0.8}Sr_{0.2}Co_{0.2}Fe_{0.8}O_{3-\delta}$ and $La_{0.6}Sr_{0.4}Co_{0.2}Fe_{0.8}O_{3-\delta}$ (Fig. 8a) is related to the formation of oxygen vacancies and recombination effect. This hypothesis will be subsequently confirmed by the results of the isothermal measurements of the electrical conductivity and thermoelectric power, as a function of the oxygen partial pressure under the conditions of thermodynamical equilibrium. Fig. 10 shows the electrical conductivity and thermoelectric power of $La_{0.8}Sr_{0.2}Co_{0.2}Fe_{0.8}O_{3-\delta}$, as a function of the oxygen partial pressure for a few chosen temperatures. It can be seen that at 650 °C the defects in the oxygen sublattice have not been formed yet. A distinct change in the conductivity and thermoelectric power, resulting from changes in the oxygen partial pressure and indicating the oxygen vacancies formation is observed above 800 °C. This is a so called Tamman temperature, i.e. above this temperature defects resulting from the deviation from stoichiometry are formed. The analogous dependencies for a perovskite oxide with higher strontium content $La_{0.6}Sr_{0.4}Co_{0.2}Fe_{0.8}O_{3-\delta}$ are exemplified in Fig. 11. A noticeable difference exists between the values of the electrical conductivity and thermoelectric power measured as a function of the oxygen partial pressure for the compositions: $La_{0.8}Sr_{0.2}Co_{0.2}Fe_{0.8}O_{3-\delta}$ and $La_{0.6}Sr_{0.4}Co_{0.2}Fe_{0.8}O_{3-\delta}$ (see Figs. 10 and 11). With the increasing strontium content the electrical conductivity and thermoelectric power undergo distinct changes with varying oxygen partial pressures already at 650 °C. This signifies the growing concentration of oxygen vacancies, owing to the instability of Fe^{4+} in a perovskite-type structure. It is noteworthy that the obtained dependencies between the electrical conductivity, thermoelectric power and the oxygen partial pressure (Figs. 10 and 11) are unusual for a nonstoichiometric oxide. For perovskite type oxides, a decrease of the oxygen partial pressure results in an increase of the oxygen vacancies concentration, according to the relation $[Vo^{\bullet\bullet}] \sim pO_2^{-1/n}$ ($n = 6$), which can be derived on the basis of the point defects

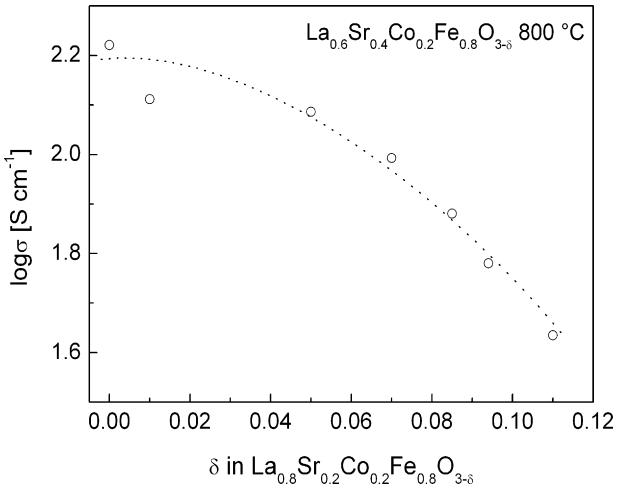

Fig. 12. Relationship between the electrical conductivity and the concentration of oxygen vacancies for $La_{0.6}Sr_{0.4}Co_{0.2}Fe_{0.8}O_{3-\delta}$ perovskite (oxygen nonstoichiometry data from [71]).

theory. On the contrary, the exponent calculated for the relationship between the conductivity and the oxygen partial pressure (Fig. 11a) is of the opposite sign ($\sigma \sim pO_2^{1/n}$). Therefore, with the growing concentration of the oxygen vacancies the electrical conductivity decreases, which was demonstrated for the experimental relationship between the electrical conductivity and the concentration of oxygen vacancies (donors) (Fig. 12). It can be seen that the electrical conductivity decreases with a growing deviation from stoichiometry. Consequently, the electrons originating from the ionization of donors (i.e. oxygen vacancies) are unable to reach the conductivity band and recombine with holes in the valence band (effective carriers), causing a decrease in their concentration. As a result, the thermoelectric power of $La_{0.6}Sr_{0.4}Co_{0.2}Fe_{0.8}O_{3-\delta}$ is of a positive sign and is lower than for $La_{0.8}Sr_{0.2}Co_{0.2}Fe_{0.8}O_{3-\delta}$ (Fig. 8b). The process can be described by the following equations:

$$O_O = V_O^{\bullet\bullet} + 2e^- + 1/2O_2, \qquad 2M^{m+} + 2e^- = 2M^{(m-1)+}$$

The recombination process is responsible for the observed drop in electrical conductivity for both the materials at high temperatures (Fig. 8a); an increase in the oxygen vacancies concentration and a decrease in concentration of the effective electronic charge carriers. Moreover, for the studied materials, $La_{0.8}Sr_{0.2}Co_{0.2}Fe_{0.8}O_{3-\delta}$ and $La_{0.6}Sr_{0.4}Co_{0.2}Fe_{0.8}O_{3-\delta}$ the electronic component of the electrical conductivity is much higher than the ionic component.

Fig. 13 presents thermal dependencies of the electrical conductivity and thermoelectric power of the perovskites from the LSCFN group: $LaCo_{1/3}Fe_{1/3}Ni_{1/3}O_{3-\delta}$ and $La_{0.9}Sr_{0.1}Co_{1/3}Fe_{1/3}Ni_{1/3}O_{3-\delta}$, measured within the temperature range of 130–930 °C in air. The results obtained at high temperatures, i.e. at and above 500 °C correspond to the conditions of thermodynamic equilibrium. For $LaCo_{1/3}Fe_{1/3}Ni_{1/3}O_{3-\delta}$ a simple, activated mechanism of the electrical conductivity is observed. With the growing temperature the conductivity slightly decreases. For $LaCo_{1/3}Fe_{1/3}Ni_{1/3}O_{3-\delta}$ the following oxidation states should

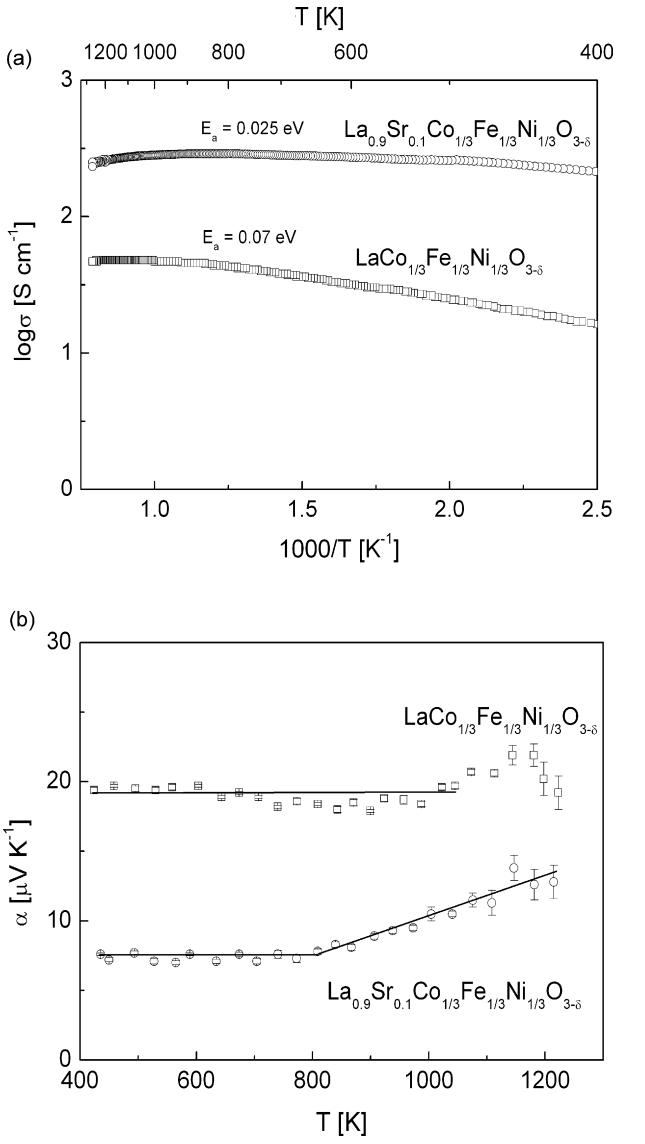

Fig. 13. Temperature dependence of (a) the electrical conductivity and (b) the thermoelectric power of $LaCo_{1/3}Fe_{1/3}Ni_{1/3}O_{3-\delta}$ and $La_{0.9}Sr_{0.1}Co_{1/3}Fe_{1/3}Ni_{1/3}O_{3-\delta}$ measured in air.

be considered: $Co^{3+}(3d^6)$, $Fe^{3+}(3d^5)$, $Ni^{3+}(3d^7)$ or $Co^{4+}(3d^5)$, $Fe^{3+}(3d^5)$, $Ni^{2+}(3d^8)$. The estimated activation energy, together with the nature of the thermal dependency of thermoelectric power indicates that the conduction occurs in more than one electronic band. The obtained activation energy of the electrical conductivity is equal to 0.07 eV and can be identified with the energy band gap between t_{2g} and e_g band (0.14 eV) (Fig. 14). The transport occurs simultaneously via holes in the t_{2g} band and the electrons in the e_g band. A substitution of La with Sr ($La_{0.9}Sr_{0.1}Co_{1/3}Fe_{1/3}Ni_{1/3}O_{3-\delta}$) leads to the enhancement of an average valency of the transition metal ions, leading in turn to improved transport properties, i.e. an increase in the electrical conductivity of one order of magnitude (Fig. 13a). Also, one can note that for the composition $La_{0.9}Sr_{0.1}Co_{1/3}Fe_{1/3}Ni_{1/3}O_{3-\delta}$ the activation energy of the electrical conductivity is diminished, therefore the energy split between the t_{2g} and e_g bands equal 0.05 eV. This can be associated with the observed

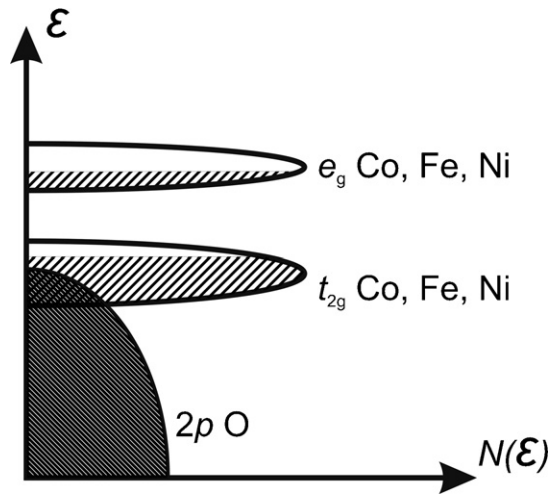

Fig. 14. Schematic representation of the electronic structure of the LSCFN perovskites.

decrease in the lattice parameter with the growing content of strontium (5.4890 Å for $LaCo_{1/3}Fe_{1/3}Ni_{1/3}O_{3-\delta}$ and 5.4828 Å for $La_{0.9}Sr_{0.1}Co_{1/3}Fe_{1/3}Ni_{1/3}O_{3-\delta}$). Above about 730 °C for both compositions a decrease in the electrical conductivity with a growing temperature is observed; moreover, for $La_{0.9}Sr_{0.1}Co_{1/3}Fe_{1/3}Ni_{1/3}O_{3-\delta}$ a drop in the electrical conductivity is more significant. This behavior can be accounted for by the results of the electrical conductivity and thermoelectric power measurements for both compositions. The measurements were carried out at a varying oxygen partial pressure and at a constant temperature, under the conditions of thermodynamic equilibrium (Figs. 15 and 16). By comparing the results obtained for $LaCo_{1/3}Fe_{1/3}Ni_{1/3}O_{3-\delta}$ and $La_{0.9}Sr_{0.1}Co_{1/3}Fe_{1/3}Ni_{1/3}O_{3-\delta}$ one should note significant differences between the structures of ionic defects, related to the oxygen nonstoichiometry. The electrical conductivity and thermoelectric power for $LaCo_{1/3}Fe_{1/3}Ni_{1/3}O_{3-\delta}$ practically do not depend on the oxygen partial pressure up to 800 °C, denoting that the oxygen is immobilized in the lattice within this range of temperatures. The Tamman temperature for $LaCo_{1/3}Fe_{1/3}Ni_{1/3}O_{3-\delta}$ is of the order of 900 °C. A substitution of some lanthanum by strontium (0.1 mol per mole) leads to an increase in the concentration of oxygen vacancies, which is reflected by a strong correlation between the electrical conductivity and thermoelectric power and oxygen partial pressure (Fig. 16). A plausible explanation behind the increasing oxygen nonstoichiometry prior to introducing Sr^{2+} ions to $LaCo_{1/3}Fe_{1/3}Ni_{1/3}O_{3-\delta}$ structure is, that it is difficult to acquire a higher valency in case of the transition metal ions. In $LaCo_{1/3}Fe_{1/3}Ni_{1/3}O_{3-\delta}$, corresponding oxidation states of the transition metal ions are Co^{3+}, Fe^{3+}, Ni^{3+} or Co^{4+}, Fe^{3+}, Ni^{2+}. Introducing Sr^{2+} would require a higher valency of iron, from Fe^{3+} to Fe^{4+}, which is unstable in this structure. The resulting changes in the electrical conductivity and thermoelectric power in function of oxygen partial pressure (Figs. 15 and 16) are analogous to the previously discussed oxides of a perovskite type, belonging to the LSCF group. Hence, the deviation from stoichiometry towards oxygen deficiency causes a decrease in the concentration of the effective

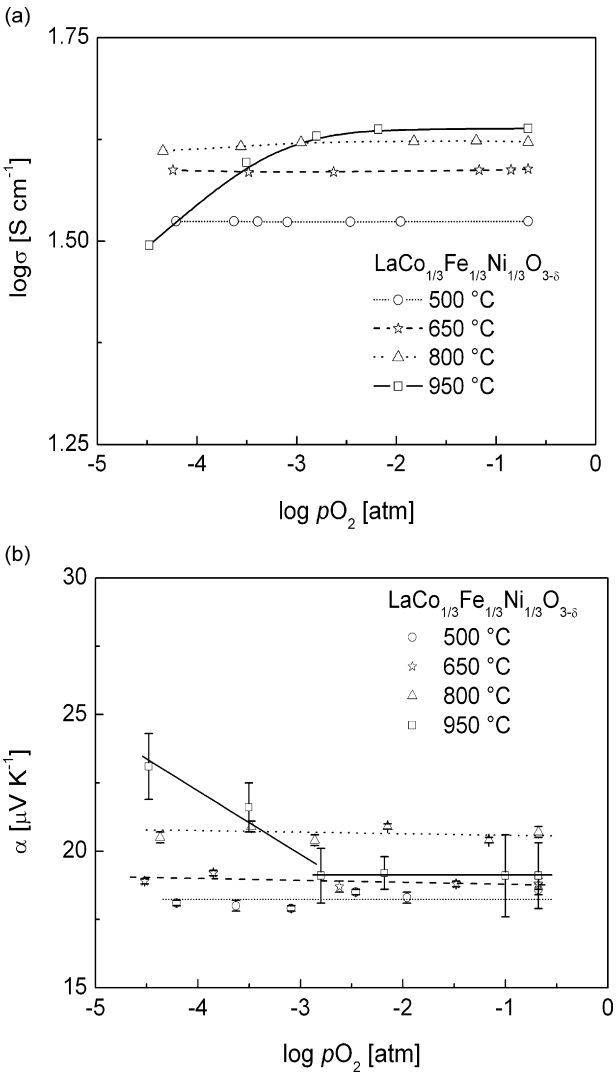

Fig. 15. Equilibrium dependences of (a) the electrical conductivity and (b) the thermoelectric power of $LaCo_{1/3}Fe_{1/3}Ni_{1/3}O_{3-\delta}$ as a function of the oxygen partial pressure.

electronic charge carriers. At high temperatures, the drop in the electrical conductivity observed for both the materials (Fig. 13a) can be ascribed to a recombination effect (the increase of the oxygen vacancies concentration with the growing temperature and, concomitantly, the decreasing concentration of the electronic charge carriers). Similarly to LSCF group in the case of the perovskites from LSCFN group the electronic component of the electrical conductivity is much higher than the ionic component.

The enhanced efficiency of SOFC, apart from the modification of the chemical composition and ionic defects structure of the cathode materials, can be achieved by the optimization of the electrode microstructure. For the cathode material, it is vital to increase the surface area of the interface between the electrode and the electrolyte. In practice, one or more layers of a mixed composition are introduced between the electrode and the electrolyte. For a certain cathode material, the feasibility of technological applications, apart from transport and catalytic properties previously described, is also related to other important features of the material. In particular, a thermal and

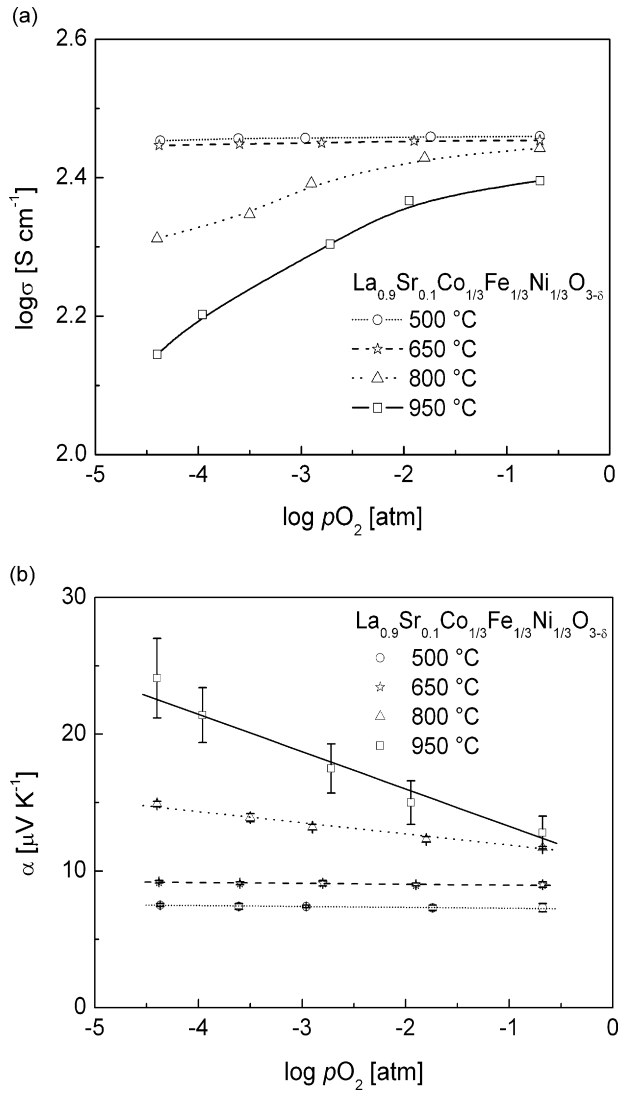

Fig. 16. Equilibrium dependences of (a) the electrical conductivity and (b) the thermoelectric power of $La_{0.9}Sr_{0.1}Co_{1/3}Fe_{1/3}Ni_{1/3}O_{3-\delta}$ as a function of the oxygen partial pressure.

chemical resistance, mechanical stability of the porous structure, non-reactivity towards the electrolyte, matching of the thermal expansion coefficients of a cathode, an electrolyte and an interconnector; finally, a good adhesion between the cathode and electrolyte are crucial for the successful implementation in SOFC. Problems concerning the industrial fabrication are of the equal importance, especially simplified methods of manufacturing, repeatability of the synthesis process and the design of the microstructure, as well as economical and ecological aspects of the technology.

2.3. Anode materials

In the earliest solutions for SOFC, single-phase materials were used as anodes, such as graphite, iron oxide, platinum metals or transition metals. Unfortunately, these materials were highly susceptible to corrosion and degradation processes and suffered from a mismatch of the thermal expansion coefficients between the anode and zirconia electrolyte. Furthermore, the combustion process of the fuel proceeded only at the three-phase boundary: gas–electrode–electrolyte. The Ni/YSZ cermet has been used as the anodic material for SOFC for over 30 years [72–74]. This material exhibits a mixed ionic–electronic conductivity, favoring the combustion of the fuel practically in the whole volume of the porous anode. The ionic conductivity results from oxygen ions transport via oxygen vacancies in YSZ. The electronic component of conductivity is related to the presence of the metallic nickel in the anodic material. For 30% of Ni a percolation path is formed, leading, in a microscopic scale, to metallic properties of the anodic material. Simultaneously the coefficient of thermal expansion of the cermet towards the electrolyte is only slightly altered. Metallic nickel is an excellent catalyst for hydrogen oxidation; it also catalyses the reforming of methane with steam. A survey over the Ni/YSZ system under the operating conditions of a cell [6] indicated the necessity of a further optimization of the microstructure. The passage of the electric current leads to nickel agglomeration, leading in turn to a serious decrease the electrochemical efficiency of the anode. Nickel has also another serious drawback, because of its quite high catalytic activity towards cracking of higher hydrocarbons, what in turn leads to carbon deposition and lowers effectiveness of anode process in the cell. Therefore, new anodic materials of a cermet type are explored, less active towards cracking of hydrocarbons. For the latest technological solutions, cermets such as Cu/CeO_2, Cu/CeO_2/YSZ were proposed [73]. CeO_2 plays the role of a catalyst in the fuel oxidation process and prevents the release of carbon. The application of a ceria-based cermet has a major drawback arising from the lattice expansion, which occur at a low oxygen partial pressure. This is accompanied by the reduction of Ce^{4+} to Ce^{3+}. Investigations [73] indicate that a heavy doping with the ions of lower valency, such as Sm^{3+} or Gd^{3+} up to $Ce_{0.6}Sm_{0.4}O_2$ composition effectively eliminates this effect, while the electrical conductivity is only slightly decreased. These results are consistent with our work [27].

The results found in literature show that, in the case of hydrocarbons oxidation processes, the efficiency of the anodic reaction is insufficient. The oxidation reaction of hydrocarbons is affected by the pressure of the water steam, depending on the rate of the processes occurring in the cell. As far, the mechanism of this oxidation reaction has not been fully explored. Knowledge of the catalytic mechanism of the oxidation reaction of hydrocarbons is of key importance for designing the anodic material characterized by a high efficiency. However, it involves measuring techniques which pose technical difficulties, such as Raman spectroscopy or IR spectroscopy carried in situ under operating conditions of the cell.

Potential candidates for anodic materials are transition metal oxides which belong to perovskite group, described by the formula $La_{1-x}Sr_xCrO_{3-\delta}$. So far, these compounds were used as interconnectors for SOFC. They show a mixed electronic–ionic conductivity, which is essential for the anode material, and are stable at low oxygen partial pressures. Transport and catalytic properties of these materials are usually modified by substituting chromium with other transition metals: $La_{1-x}Sr_xCr_{1-y}M_yO_{3-\delta}$

(M = Mn, Fe, Co, Ni). However, an extended research over the optimization of chemical composition and microstructure, as well as maximizing the electronic conductivity and enhancing the chemical stability in reductive atmospheres is necessary.

3. Conclusions

The future of SOFC is associated with the reduction of the working temperature down to about 600–700 °C. Innovative technologies must be implemented in order to produce the electrode and electrolyte materials working effectively within the desirable temperature range. This requires the development of new electrolytes and electrode materials, operating effectively at these temperatures. Designing and modelling the functional properties of the oxide electrolytes and electrode materials characterized by a high catalytic activity is possible on the basis of the theory of nonstoichiometric defects and the analysis of their electronic structure. The functional gradient junctions between the cathode and the electrolyte may help in decreasing the electrical resistance of the interface and in mutual matching of the thermal expansion coefficients.

Acknowledgement

This work was financially supported by a Polish Committee for Science KBN under the grant no. PBZ-100/1/3/2004.

References

[1] M. Dokiya, Solid State Ionics 383 (2002) 152.
[2] O. Yamamoto, Electrochim. Acta 45 (2000) 2423.
[3] S.P.S. Badwal, K. Foger, Ceram. Int. 22 (1996) 257.
[4] N.Q. Minh, J. Am. Ceram. Soc. 76 (1993) 563.
[5] G.A. Tompsett, C. Finnerty, K. Kendall, T. Alston, N.M. Sammes, J. Power Sources 86 (2000) 376.
[6] E. Ivers-Tiffee, A. Weber, D. Herbstritt, J. Eur. Ceram. Soc. 21 (2001) 1805.
[7] T. Takahashi (Ed.), B.C.H. Steele in High Conductivity Solid Ionic Conductors, World Scientific Singapore, 1989.
[8] P. Huang, A. Petric, J. Electrochem. Soc. 143 (1996) 1644.
[9] D. Lee, I. Lee, Y. Jeon, R. Song, Solid State Ionics 176 (2005) 1021.
[10] S. Zha, C. Xia, G. Meng, J. Power Sources 115 (2003) 44.
[11] J. Gong, Y. Li, Z. Tang, Y. Xie, Z. Zhang, Mater. Chem. Phys. 76 (2002) 212.
[12] S. Nakayama, M. Sakamoto, 18 (1998) 1413.
[13] T.Q. Ta, T. Tsuji, Y. Yamamura, J. Alloys Compd. 408–412 (2006) 253.
[14] Y. Arachi, H. Sakai, O. Yamamoto, Y. Takeda, N. Imanishai, Solid State Ionics 121 (1999) 133.
[15] T.H. Etsell, S.N. Flengas, Chem. Rev. 70 (1970) 339.
[16] C. Haering, A. Roosen, H. Schichl, M. Schnfller, Solid State Ionics 176 (2005) 261.
[17] S.P.S. Badwal, F.T. Ciacchi, S. Rajendran, J. Drennan, Solid State Ionics 109 (1998) 167.
[18] L.R. Pederson, P. Singh, X.-D. Zhou, Vacuum 80 (2006) 1066.
[19] Y. Ji, J. Liu, Z. Lu, X. Zhao, T. He, W. Su, Solid State Ionics 126 (1999) 277.
[20] H. Inaba, H. Tagawa, Solid State Ionics 83 (1996) 1.
[21] T. Mori, T. Ikegami, H. Yamamura, J. Electrochem. Soc. 146 (1999) 4380.
[22] H. Yahiro, T. Ohuchi, K. Eguchi, H. Arai, J. Mater. Sci. 23 (1988) 1036.
[23] H. Yahiro, K. Eguchi, H. Arai, Solid State Ionics 36 (1989) 71.
[24] K. Eguchi, T. Setoguchi, T. Inoue, H. Arai, Solid State Ionics 52 (1992) 165.
[25] M. Dudek, J. Molenda, Ceramics 84 (2004) 177.
[26] F.-Y. Wang, S. Chen, S. Cheng, Electrochem. Commun. 6 (2004) 743.
[27] J. van Herle, D. Seneviratne, A.J. McEvoy, J. Eur. Ceram. Soc. 19 (1999) 837.
[28] N.V. Skorodumova, S.I. Simak, B.I. Lundqvist, I.A. Abrikosov, B. Johansson, Phys. Rev. Lett. 89 (16) (2002) 166601.
[29] D. Hirabayashi, A. Tomita, S. Teranishi, T. Hibino, M. Sanoc, Solid State Ionics 176 (2005) 881.
[30] K. Eguchi, T. Setoguchi, T. Inoue, H. Aral, Solid State Ionics 52 (1992) 165.
[31] A. Tschöpe, E. Sommer, R. Birringer, Solid State Ionics 139 (2001) 255.
[32] A. Tschöpe, Solid State Ionics 139 (2001) 267.
[33] I. Kosacki, H.U. Anderson, Y. Mizutani, K. Ukai, Solid State Ionics 152/153 (2002) 431.
[34] I. Kosacki, NATO Science Series, Fuel Cell Technologies—State and Perspectives, Springer, 2005, pp. 395.
[35] I. Kosacki, Chemical Letters, Wroclaw, 2005, pp. 77.
[36] V. Thangadurai, W. Weppner, Electrochim. Acta 50 (2005) 1871.
[37] X. Zhang, S. Ohara, R. Maric, H. Okawa, T. Fukui, H. Yoshida, T. Inagaki, K. Miura, Solid State Ionics 133 (2000) 153.
[38] K. Yamaji, T. Horita, M. Ishikawa, N. Sakai, H. Yokokawa, Solid State Ionics 121 (1999) 217.
[39] J. Yan, H. Matsumoto, M. Enoki, T. Ishihara, Electrochem. Sol. -St. Lett. 8 (2005) A389.
[40] V.V. Kharton, A.L. Shaula, M.V. Patrakeev, J.C. Waerenborgh, D.P. Rojas, N.P. Vyshatko, E.V. Tsipis, A.A. Yaremchenko, F.M.B. Marques, J. Electrochem. Soc. 151 (2004) A1236.
[41] A. Najib, J.E.H. Sansom, J.R. Tolchard, P.R. Slater, M.S. Islam, Dalton Trans. (2004) 3106.
[42] C.E. Mohn, N.L. Allan, C.L. Freeman, P. Ravindran, S. Stølen, J. Sol. St. Chem. 178 (2005) 346.
[43] A. Rolle, R.N. Vannier, N.V. Giridharan, F. Abraham, Solid State Ionics 176 (2005) 2095.
[44] S.J. Skinner, Fuel Cells Bull. 339 (2001) 6.
[45] S. Stølen, E. Bakkenw, Ch.E. Mohn, Phys. Chem. Chem. Phys. 8 (2006) 429.
[46] L.-W. Tai, M.N. Nasrallah, H.U. Anderson, D.M. Sparlin, S.R. Sehlin, Solid State Ionics 76 (1995) 273.
[47] L.-W. Tai, M.N. Nasrallah, H.U. Anderson, D.M. Sparlin, S.R. Sehlin, Solid State Ionics 76 (1995) 259.
[48] S. Li, W. Jin, N. Xu, J. Shi, Solid State Ionics 124 (1999) 161.
[49] H.Y. Tu, Y. Takeda, N. Imanishi, O. Yamamoto, Solid State Ionics 117 (1999) 277.
[50] G.C. Kostogloudis, C. Ftikos, Solid State Ionics 126 (1999) 143.
[51] D. Waller, J.A. Lane, J.A. Kilner, B.C.H. Steele, Mater. Lett. 27 (1995) 225.
[52] D. Waller, J.A. Lane, J.A. Kilner, B.C.H. Steele, Solid State Ionics 86–88 (1996) 767.
[53] M.B. Phillips, N.M. Sammes, O. Yamamoto, Solid State Ionics 123 (1999) 131.
[54] Y. Takeda, Y. Sakaki, T. Ichikawa, N. Imanishi, O. Yamamoto, M. Mori, N. Mori, T. Abe, Solid State Ionics 72 (1994) 257.
[55] R. Chyba, F. Yoshimura, Y. Samurai, Solid State Ionics 124 (1999) 281.
[56] R. Chyba, F. Yoshimura, Y. Samurai, Solid State Ionics 152/153 (2002) 575.
[57] M. Hrovat, N. Katsarakis, K. Reichmann, S. Bernik, D. Kuscer, J. Holc, Solid State Ionics 83 (1996) 99.
[58] E. Maguire, B. Gharbage, F.M.B. marques, J.A. Labrincha, Solid State Ionics 127 (2000) 329.
[59] Z.P. Shao, C. Kwak, S.M. Haile, Solid State Ionics 175 (2004) 39.
[60] Z. Shao, S.M. Haile, J. Ahn, P.D. Ronney, Z. Zhan, S.A. Barnett, Nature 9 (2005) 795.
[61] Proceedings of the "15th International Conference on Solid State Ionics", Baden–Baden, Germany, July 17–22, 2005.
[62] Q.L. Liu, K.A. Khor, S.H. Chan, J. Power Sources 161 (2006) 123.
[63] K. Huang, H.Y. Lee, J.B. Goodenough, J. Electrochem. Soc. 145 (1998) 3220.
[64] U. Russo, L. Nodari, M. Faticanti, V. Kuncser, G. Filoti, Solid State Ionics 176 (2005) 97.

[65] K. Świerczek, J. Marzec, D. Pałubiak, W. Zając, J. Molenda, Solid State Ionics 177 (2006) 1811.
[66] J. Molenda, A. Kubik, Solid State Ionics 117 (1999) 57.
[67] J. Molenda, J. Marzec, K. Świerczek, W. Ojczyk, M. Ziemnicki, M. Molenda, M. Drozdek, R. Dziembaj, Solid State Ionics 171 (2004) 215.
[68] J. Molenda, A. Stokłosa, W. Znamirowski, Phys. Stat. Sol. 142 (1987) 517.
[69] J. Molenda, High Temp. Mater. Process. 10 (1992) 223.
[70] J. Molenda, I. Nowak, L. Jedynak, J. Marzec, A. Stokłosa, Solid State Ionics 135 (2000) 235.
[71] J.W. Stevenson, T.R. Armstrong, R.D. Carneim, L.R. Pederson, W.J. Weber, J. Electrochem. Soc. 143 (1996) 2722.
[72] H.S. Spacil, US Patent 3,558,360 (1970).
[73] S.D. Park, J.M. Vohs, R.J. Gorte, Nature 404 (2000) 265.
[74] A. Atkinson, S. Barnett, R.J. Gorte, J.T.S. Irvine, A.J. McEvoy, M. Mogensen, S.C. Singhal, J. Vohs, Nat. Mater. (2004) 3.